

Neurite Extension and Orientation of Spiral Ganglion Neurons Can Be Directed by Superparamagnetic Iron Oxide Nanoparticles in a Magnetic Field

Yangnan Hu,^{1,*} Dan Li,^{2,*}
Hao Wei,^{3,*} Shan Zhou,¹
Wei Chen,¹ Xiaoqian Yan,¹
Jaiying Cai,¹ Xiaoyan Chen,¹
Bo Chen,⁴ Menghui Liao,¹
Renjie Chai,^{1,5}
Mingliang Tang^{1,5,6}

¹State Key Laboratory of Bioelectronics, School of Life Sciences and Technology, Jiangsu Province High-Tech Key Laboratory for Bio-Medical Research, Southeast University, Nanjing, 210096, People's Republic of China; ²School of Biology, Food and Environment, Hefei University, Hefei, 230601, People's Republic of China; ³Department of Otorhinolaryngology Head and Neck Surgery, Drum Tower Clinical Medical College, Nanjing Medical University, Nanjing, 210000, People's Republic of China; ⁴Materials Science and Devices Institute, Suzhou University of Science and Technology, Suzhou, 215009, People's Republic of China; ⁵Co-innovation Center of Neuroregeneration, Nantong University, Nantong, 226001, People's Republic of China; ⁶Department of Cardiovascular Surgery of the First Affiliated Hospital & Institute for Cardiovascular Science, Medical College, Soochow University, Suzhou, 215000, People's Republic of China

*These authors contributed equally to this work

Correspondence: Renjie Chai;
Mingliang Tang
Email renjiec@seu.edu.cn;
mltang@suda.edu.cn

Introduction: Neuroregeneration is a major challenge in neuroscience for treating degenerative diseases and for repairing injured nerves. Numerous studies have shown the importance of physical stimulation for neuronal growth and development, and here we report an approach for the physical guidance of neuron orientation and neurite growth using superparamagnetic iron oxide (SPIO) nanoparticles and magnetic fields (MFs).

Methods: SPIO nanoparticles were synthesized by classic chemical co-precipitation methods and then characterized by transmission electron microscope, dynamic light scattering, and vibrating sample magnetometer. The cytotoxicity of the prepared SPIO nanoparticles and MF was determined using CCK-8 assay and LIVE/DEAD assay. The immunofluorescence images were captured by a laser scanning confocal microscopy. Cell migration was evaluated using the wound healing assay.

Results: The prepared SPIO nanoparticles showed a narrow size distribution, low cytotoxicity, and superparamagnetism. SPIO nanoparticles coated with poly-L-lysine could be internalized by spiral ganglion neurons (SGNs) and showed no cytotoxicity at concentrations less than 300 $\mu\text{g/mL}$. The neurite extension of SGNs was promoted after internalizing SPIO nanoparticles with or without an external MF, and this might be due to the promotion of growth cone development. It was also confirmed that SPIO can regulate cell migration and can direct neurite outgrowth in SGNs preferentially along the direction imposed by an external MF.

Conclusion: Our results provide a fundamental understanding of the regulation of cell behaviors under physical cues and suggest alternative treatments for sensorineural hearing loss caused by the degeneration of SGNs.

Keywords: physical cues, neurites orientation, hearing loss, cochlear implants, migration

Introduction

Within the mammalian auditory system, spiral ganglion neurons (SGNs) are the primary neurons that convey sound information from mechanosensory hair cells residing in the inner ear to the cochlear nuclei in the brainstem.¹ Hair cell loss leading to degeneration of SGNs is the primary cause of sensorineural hearing loss, but SGNs can also degenerate due to acoustic overexposure,^{2,3} ototoxic drugs,^{4,5} and aging.^{6,7} In general, without external intervention, the loss of SGNs and auditory nerve fibers is irreversible in the adult ear, which leads to permanent sensorineural hearing loss.

Therefore, SGNs are potential targets for protection and regenerative therapies.⁸ In addition to pharmacological methods of hearing loss treatment, cochlear implants (CIs) are effective clinical options for partially restoring hearing in patients with hearing loss. However, the functional principle of CIs is the direct electrical stimulation of SGNs, and this means that the effectiveness of CIs primarily depends on the remaining SGNs.^{6,7} Another factor limiting the effectiveness of CIs is the anatomical gap that exists between the electrode array and the SGNs, leading to a current spread with unspecific stimulation.^{9–12} One of the potential solutions for this is to direct the neurites of the SGNs to grow towards the stimulating electrodes.¹³ Thus, it is essential to maintain and promote the survival and neurite growth of SGNs and guide them towards the target to improve CI performance in sensorineural hearing loss patients.

There is a growing body of evidence indicating that physical stimuli are a crucial factor in neuronal growth and development,^{14,15} and individual cells like neurons can sense and respond to the mechanics of their environment.^{16,17} In recent years, magnetic nanoparticles have been widely used in the biomedical field for magnetic resonance imaging (MRI),^{18–20} cell-labeling,^{21,22} and targeted drug or gene delivery.²³ Magnetic iron oxides such as Fe₃O₄ and α -Fe₂O₃ nanoparticles are the most studied particles for these applications because of their high magnetization under magnetic fields,^{24–26} their high stability, and their biological compatibility.^{27,28} More importantly, recent studies have demonstrated the ability of superparamagnetic iron oxide (SPIO) nanoparticles to direct neurite orientation.^{29,30}

In the present study, we sought to demonstrate the potential of SPIO nanoparticles and magnetic fields (MFs) to regulate SGNs, especially with regards to neuronal orientation and neurite growth.

Materials and Methods

Synthesis and Characterization of SPIO Nanoparticles

The SPIO nanoparticles used in this study were synthesized by classic chemical co-precipitation methods as described previously.³¹ Briefly, an aqueous solution (10 mL) of polyglucose sorbitol carboxymethyl ether (PSC, 200 mg) was aerated with nitrogen for 5 min to remove oxygen. Next, 30 mg FeCl₂ (0.236 mmol) and 60 mg FeCl₃ (0.37 mmol) were completely dissolved in 15 mL deionized water, and the mixture was added to the PSC solution. Subsequently, 1 g ammonium hydroxide (28% w/v) was rapidly added to the

mixed solution and vigorously mechanically stirred in a water bath at 80°C for 30 min. Finally, the iron oxide nanoparticles were collected using an ultrafiltration centrifuge tube and washed with ultrapure water several times. The morphology and size of the prepared SPIO nanoparticles were determined using a transmission electron microscope (TEM; JEM-2100, JEOL, Japan) and dynamic light scattering. The magnetic properties of the SPIO nanoparticles were determined at 37°C using a vibrating sample magnetometer. The XRD pattern was obtained from an X-ray diffractometer (Rigaku Ultima IV, Japan). For cellular uptake of SPIO nanoparticles into SGNs, the prepared nanoparticles were coated with poly-L-lysine (Sigma, USA) in an ultrasonic bath.

Animals

All animal protocols were approved by the Institution Animal Care and Use Committee of Southeast University, and all animals were treated following the National Institutes of Health Guide for the Care and Use of Laboratory Animals. All of the FVB mice were raised in-house under a 12:12 h light-dark cycle. All efforts were made to minimize the number of animals used and to reduce their suffering.

Isolation and Culture of Mouse SGNs

To obtain SGNs, postnatal day 2 or 3 mice were decapitated and the temporal bone was dissected out after removal of the brain and immersed in ice-cold sterile Hanks' balanced salt solution (HBSS; Gibco, USA). The cochleae were isolated from the temporal bone in HBSS under a dissecting microscope (Leica, Germany), and the bony shell was sheared off and the stria vascularis and the organ of Corti were removed. The modiolus was collected and placed in 0.1% trypsin (Gibco, USA) to digest for 10 min at 37°C. Soybean trypsin inhibitor (Gibco, USA) was added to stop the digestion. Cells were separated by gently pipetting up and down 80–100 times with blunt tips, and the solution was percolated through a 40 μ m cell strainer (Falcon, USA) to obtain a single-cell suspension. Before cell seeding, the coverslips were coated with laminin (Sigma, USA) in phosphate-buffered saline (PBS; Gibco, USA) overnight at 37°C and then washed with PBS. SGNs were plated on laminin-coated coverslips and cultured at 37°C in a 5% CO₂ humidified incubator for future experiments. For the first 24 hours, SGNs were cultured with SGN1 medium consisting of DMEM/F12 (Gibco, USA), 5% fetal bovine serum (Invitrogen, USA), and ampicillin (50 μ g/mL; Sigma, USA). For long-term culture, the SGN1 medium was replaced with SGN2 medium containing DMEM/F12, N2 (Invitrogen, USA), B27 (Invitrogen, USA), EGF (20 ng/mL,

Peprtech, USA), FGF (20 ng/mL, Peprtech, USA), IGF (50 ng/mL, Peprtech, USA), HSP (20 ng/mL, Sigma, USA), and ampicillin (50 µg/mL, Sigma, USA).

Magnetic Field (MF)

The MF was generated by two rectangular neodymium magnets. The magnets were positioned parallel to the box on both sides of it, and the 35 mm dish was placed in the middle of the box ([Figure S1](#), [Supporting Information](#)). We considered that the most central area of the culture dish with a diameter of 10 mm receives approximately the same MF intensity and direction. The MF intensity of the central area was adjusted by using different sized magnets. The MF intensity formed by the magnets was measured with a Tesla meter (HT20).

Cell Viability Evaluation

The cytotoxicity of the prepared SPIO nanoparticles and MF was determined using the Cell Counting CCK-8 Kit (Beyotime, China) and the LIVE/DEAD Viability/Cytotoxicity Kit (Invitrogen, USA). In the CCK-8 assay, SGNs were seeded in a 96-well plate coated with laminin at a concentration of 1×10^4 cells/well. After adhesion, the cells were exposed to the SPIO nanoparticles (concentrations of 0, 50, 100, 200, 300, and 500 µg/mL) for 6, 24, and 36 h. After washing three times with culture medium, the cells were kept in the dark with 10 µL CCK-8/200 µL fresh medium in each well for 30 min at 37°C, and a microtiter plate reader (Bio-Rad) was used to measure the absorbance at 450 nm to evaluate relative cell viabilities. In the LIVE/DEAD assay, SGNs were seeded on coverslips coated with laminin for adhesion. The cells were then exposed to 100 µg/mL SPIO nanoparticles, MF (80–90 mT), or both for 3 days. Cell viability was evaluated using the LIVE/DEAD Viability/Cytotoxicity Kit according to the manufacturer's instruction. The working concentrations of calcein AM and ethidium homodimer-1 were 2 µM and 0.5 µM, respectively.

Cellular Uptake of SPIO Nanoparticles

To confirm the cellular iron uptake, SGNs were cultured with SPIO nanoparticles for 24 h for Prussian blue staining. After incubation, the SPIO nanoparticles-containing medium was removed and the SGNs were washed three times with PBS to remove as many SPIO nanoparticles as possible from the cell surface. Following fixation for 45 min in 4% paraformaldehyde at room temperature, the cells were incubated in Prussian blue staining solution

(1:1 mixture of hydrochloric acid and potassium ferrocyanide) (Sigma, USA) for 30 min to evaluate intracellular iron distribution by light microscopy (Leica). Uptake of the SPIO nanoparticles was also evaluated using fluorescence microscopic images of the cells after being incubated with the SPIO nanoparticles labeled with rhodamine B (RB-SPIO). Briefly, after incubation, washing, and fixation as above, the cells were stained with DAPI for 30 min at room temperature and finally washed three times with PBS. Confocal imaging was conducted on a Zeiss 700 laser scanning confocal microscopy (LSM700). The quantitation of SPIO uptake by SGNs was determined by the iron content of the particles in cells. The iron content was determined by inductively coupled plasma mass spectrometer (ICP-MS, Thermo).

Neurite Growth and Orientation Under an MF

SGNs were seeded in Petri dishes pre-coated with laminin, and 24 h after seeding the cells were treated with 100 µg/mL SPIO nanoparticles. When cells were treated with the MF, the Petri dish was placed in the box between the two magnets as described above. After 7 days, the neurite length and the angle between the direction of each neurite and the MF were measured. Neurite orientation was quantified as the orientation index, which was defined as $O_i = \cos(\theta)$ ($0 < \theta < \pi/2$). The analysis was performed using the Image Pro Plus software.

Immunofluorescence

After culture, the SGNs were washed with PBS once and fixed with 4% paraformaldehyde in PBS for 45 min at room temperature and then washed three times with PBS supplemented with 0.1% Triton-X100 (Solarbio, China) (PBST). The cells were then blocked in 1% bovine serum albumin (BSA; Solarbio, China) dissolved in PBS/0.1% Triton-X100/10% heat-inactivated donkey serum (Solarbio, China) for 1 h at room temperature and then incubated with primary antibodies in blocking buffer overnight at 4°C, including mouse anti-βIII-tubulin (Abcam, USA), rabbit anti-EEA1 (Abcam, USA), rabbit anti-Rab7 (CST, USA), and mouse anti-LAMP2 (CST, USA). The next day, the SGNs were washed three times with PBST. Appropriate secondary Alexa Fluor-conjugated antibodies along with DAPI or phalloidin in PBS/0.1% Triton X-100/1% BSA were incubated for 1–2 h at room temperature and then washed three times with PBST. Finally, the cells were covered with coverslips in

DAKO fluorescence mounting medium and observed under a Zeiss 700 laser scanning confocal microscopy (LSM700).

Wound Healing Assay

Cell migration was evaluated using the wound healing assay.³² In brief, SGNs were seeded in 60 mm culture dishes and grown to form cell monolayers. Then a scratch wound was created using a sterile 200 μ L pipette tip. The floating cells were washed away with PBS, followed by culture in fresh serum-free medium. Images were taken under a light microscope at 0, 12, and 24 h after scratching. The percentage of wound closure was calculated from three independent experiments.

Statistical Analysis

Confocal and bright field images of SGNs were analyzed with the ImageJ or Image Pro Plus software to evaluate the length, orientation, migration, growth cone, and synapse development of the cells. All statistical analyses were performed in GraphPad Prism, and all data are shown as the mean \pm SD. Statistical analysis was performed using one-way ANOVA followed by a Dunnett's multiple comparisons (for comparing more than two groups) or by two-tailed, unpaired Student's *t*-test (for comparing two groups). A value of $p < 0.05$ was considered statistically significant. All experiments were performed at least three times.

Results

Characterization of SPIO Nanoparticles

The SPIO nanoparticles were synthesized by coating the γ -Fe₂O₃ core with PSC. The size and morphology of the SPIO nanoparticles were determined via TEM and dynamic light scattering. The SPIO nanoparticles dispersed well without agglomeration, and the size distribution of the cores was about 6–8 nm (Figure 1A and B). The hydrodynamic size of the SPIO nanoparticles was about 21 nm (Figure 1C). The XRD patterns (Figure S2, Supporting Information) displayed the characteristic peaks, which located at 30.3, 35.7, 43.6, 53.4, 57.2 and 63.1 assigned to the (220), (311), (400), (422), (511) and (440) phases of the γ -Fe₂O₃ crystal (JCPDS: 39–1346), consistent with another study.³³ The magnetic properties of SPIO nanoparticles are crucial for investigating their combined regulation on cells after exerting MF. The vibrating sample magnetometer results demonstrated that the obtained SPIO nanoparticles possessed superparamagnetism, with a saturation magnetization of about 56 emu/g (Figure 1D).

Cellular Uptake of SPIO Nanoparticles

We next explored the uptake of SPIO nanoparticles by SGNs, and Prussian blue staining and fluorescent confocal images verified the internalization of the SPIO nanoparticles into the SGNs (Figure 2A and B). The nanoparticles accumulated in the cell body and neurites, but not in the nucleus. Next, we quantitatively assessed the internalization of SPIO with respect to the incubation time and dose by ICP-MS. We found that the amount of iron increased with the increase of incubation time and concentration of SPIO (Figure 2C), demonstrating that SGNs internalized SPIO nanoparticles in a time and dose-dependent manner.

Cell Viability Evaluation

To verify the biocompatibility of SPIO nanoparticles, a CCK-8 assay was performed with SGNs that were incubated with SPIO nanoparticles at concentrations of 0–500 μ g/mL for 6, 12, 24, and 36 h. SPIO nanoparticles concentrations of less than 300 μ g/mL showed low cytotoxicity (>80% cell viability) (Figure 3A). However, when incubated at a high concentration of 500 μ g/mL, the SPIO nanoparticles showed cytotoxic effects in SGNs. At a concentration of 100 μ g/mL, the uptake of SPIO nanoparticles was sufficient and did not have any noticeable influence on SGN viability even after 36 h further incubation, thus we used a concentration of 100 μ g/mL for all experiments. Because the subsequent experiment introduced a magnetic field, we next tested the cytotoxicity of the SPIO nanoparticles and a magnetic field separately and together (SPIO+MF) on SGNs. CCK-8 and LIVE/DEAD staining showed that SPIO, MF, and SPIO+MF did not induce obvious cell death in SGNs (Figure 3B and C), suggesting that SPIO, MF, and SPIO+MF are biocompatible and nontoxic.

Neurite Growth with SPIO, MF, and SPIO +MF

To validate our hypothesis that SPIO nanoparticles can stimulate neuronal growth and neurite orientation under an external MF, SGNs were treated with SPIO nanoparticles, MFs (20–30 mT, 50–60 mT, 80–90mT), or SPIO +MF. SGNs were harvested after 7 days in culture (DIV7) and immunostained with anti- β III tubulin (Figure 4A). Neurite length and the angle between the neurites and the MF direction were measured to compare the neurite extension and orientation capacity of SGNs in the different groups. After 7 days of culture, the SPIO and

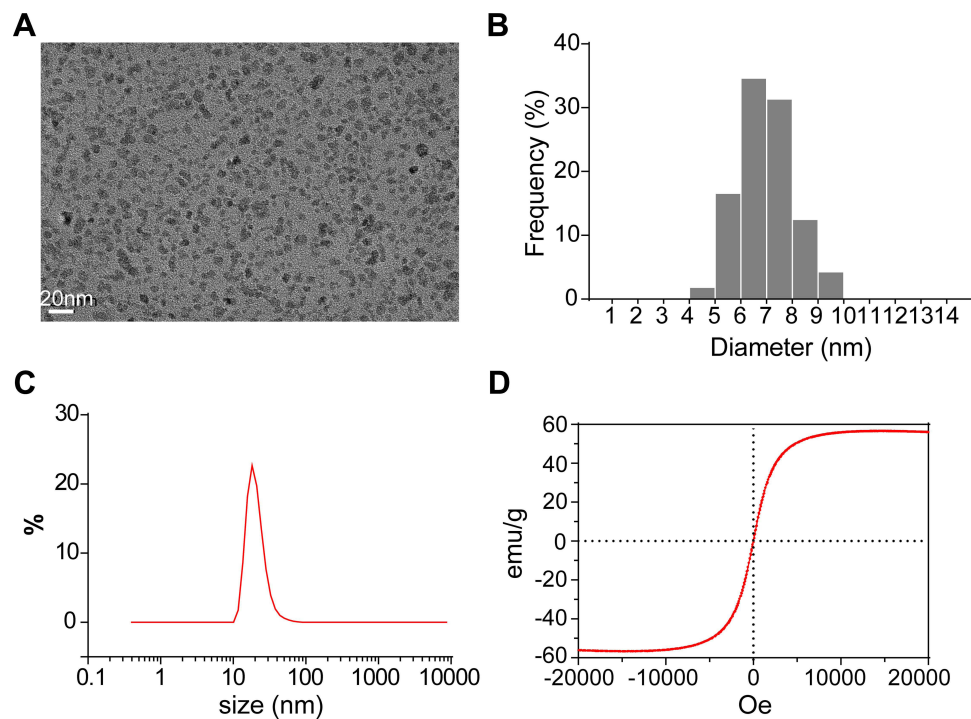


Figure 1 Characterization of the prepared SPIO nanoparticles. **(A)** TEM image of the SPIO nanoparticles. **(B)** Size distribution of SPIO nanoparticles in the TEM image. **(C)** The hydrodynamic size of the SPIO nanoparticles. **(D)** Representative magnetization curve of the SPIO nanoparticles.

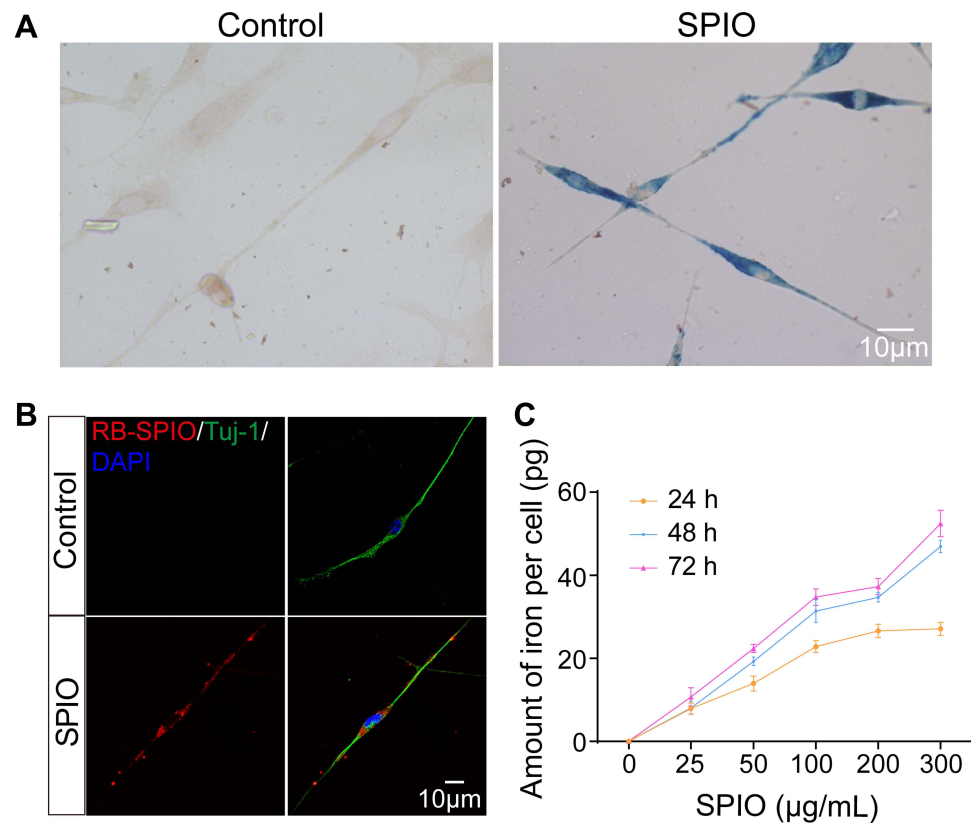


Figure 2 Internalization of SPIO nanoparticles by SGNs. **(A)** Prussian blue staining of SGNs incubated with (right) and without (left) 100 µg/mL SPIO nanoparticles for 24 h. **(B)** Representative confocal images of SGNs incubated with (bottom) and without (top) 100 µg/mL RB-SPIO nanoparticles for 24 h. **(C)** Plot of cellular uptake of SPIO nanoparticles with the incubation time and concentration, determined by ICP.

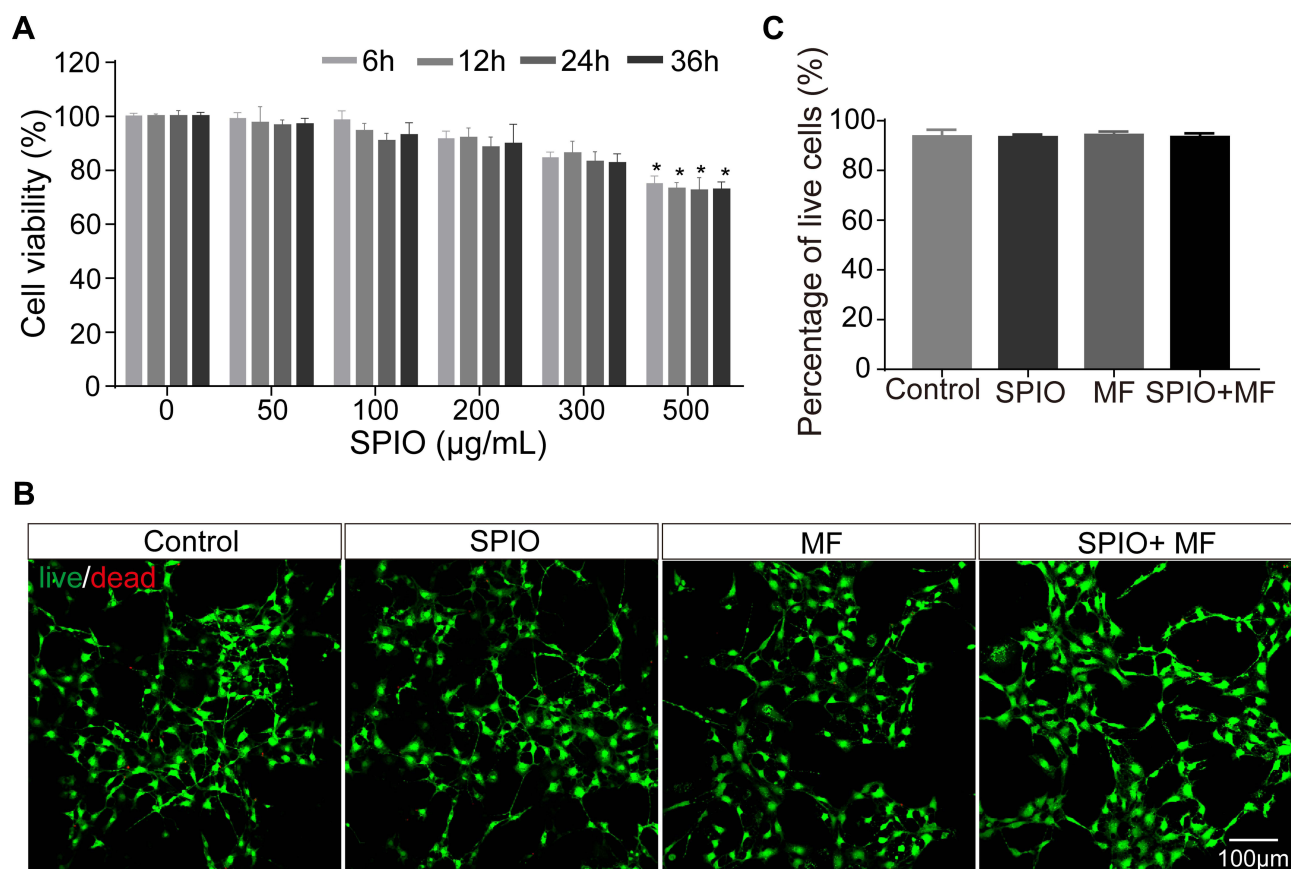


Figure 3 Cell viability of SGNs treated with SPIO nanoparticles and MF. **(A)** Cell viability results from the CCK-8 assay after incubating SGNs with 100 µg/mL SPIO nanoparticles for different times at different concentrations. * $p < 0.05$ by Student's *t*-test. **(B)** The cell viability of control SGNs and SGNs treated with SPIO nanoparticles (100 µg/mL), MF (80–90 mT), or SPIO+MF was evaluated with a LIVE/DEAD cell assay. Live cells were stained green and dead cells were stained red. **(C)** The percentage of live cells in the different groups in the LIVE/DEAD assay. One-way ANOVA showed no significant differences between groups.

SPIO+MF groups exhibited longer average neurite lengths compared to controls regardless of the MF intensity (Figure 4B and Figure S3A and S3B, S4A and S4B, Supporting Information). To quantify the orientation of the neurites, the angle between the long axis of the neurites and the direction of the MF was measured, and the orientation index was defined as $O_i = \cos\theta$ ($0 < \theta < \pi/2$). When the MF intensities were 50–60 mT and 80–90 mT, the distribution of angles between the neurite and the MF (0°) showed that the SGN neurites in the SPIO+MF group preferentially aligned along the direction of the MF, while in other groups the neurites showed a random distribution with no preferred orientation (Figure 4C and Figure S4C, Supporting Information). However, the distribution of angles between the neurite and the MF showed no preferred direction even in the SPIO+MF group when the MF intensity was 20–30 mT (Figure S3C, Supporting Information).

SPIO and SPIO+MF Promote the Development of Growth Cones

We further determined the effect of the SPIO nanoparticles and the MF on SGN growth cones and synaptic density by immunofluorescence. We stained the cultured SGNs with the neuron marker anti- β tubulin and stained the actin-supported growth cone with phalloidin at DIV3. The growth cone area of the neurites was larger, and the average filopodia length was longer when treated with SPIO or SPIO+MF compared to controls (Figure 5A, B and D). When exposed to the MF only, the growth cone area, the number of filopodia, and the average filopodia length were not significantly different compared to controls ($p > 0.05$, Figure 5B–D). The number of filopodia was not significantly different in any of the groups (Figure 5C). Collectively, our results suggest that SPIO and SPIO+MF can significantly promote the development of growth cones, which might contribute to the enhanced neurite extension.

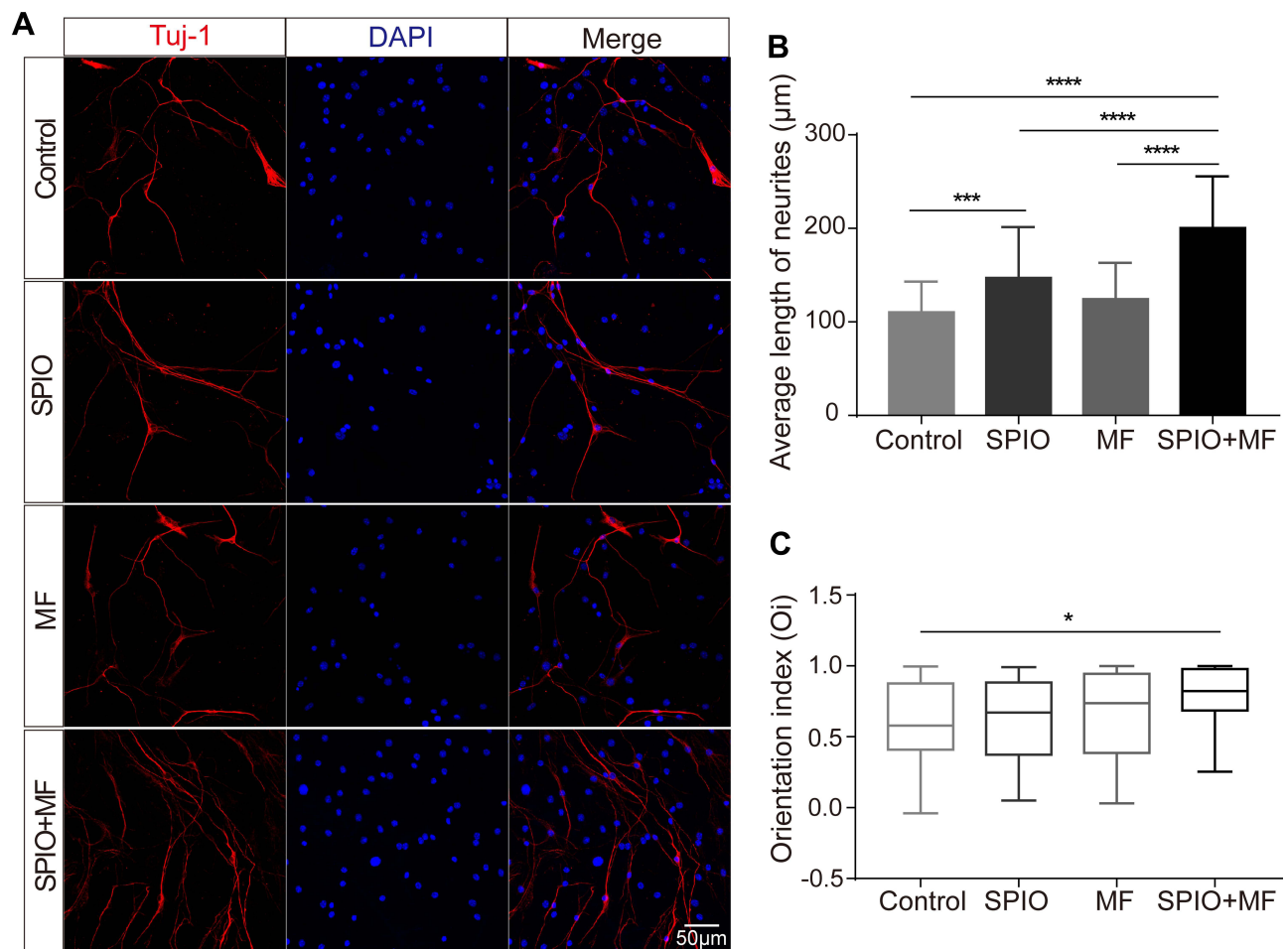


Figure 4 SPIO nanoparticles (100 µg/mL) and MF (80–90 mT) promoted the extension and orientation of SGN neurites. **(A)** Representative fluorescent images of SGNs with different treatments. **(B)** Average neurite length. *** $p < 0.001$, **** $p < 0.0001$ by one-way ANOVA. **(C)** The neurite orientation index ($\cos\theta$). $\cos = -1$ for the neurites along the direction of magnetic force. * $p < 0.05$ by one-way ANOVA.

Synapse Development

Synapses mediate the information transmission between neurons, and their structure and function directly determine neural behaviors. Therefore, the effect of the SPIO nanoparticles and the MF on synaptic density was examined at DIV14. Synapsin-1 and PSD95 have been proven to play important roles in synaptic plasticity and synapse maturation,³⁴ and the presynapses and postsynapses areas were immunostained with antibodies against the presynaptic protein synapsin-1 and the postsynaptic protein PSD95. Both low and high-magnification laser confocal microscopy showed the extensive expression of synaptic proteins and the colocalization of synapsin-1 and PSD95 in all groups (Figure 6A and B), which suggests the generation of a normal synaptic structure. In addition, there was no significant difference in the synaptic density of SGNs in the different groups (Figure 6C).

The Migratory Behavior of SGNs is Regulated by SPIO and MF

Finally, we evaluated the effects of SPIO nanoparticles and MF on SGN migration. The wound healing assay showed that SPIO nanoparticles greatly inhibited the wound closure compared with the control group. However, when an MF was applied, cell migration capacity inhibited by SPIO internalization was greatly recovered (Figure 7A and B). When only the MF acts on the SGNs, their migration capacity remains unchanged.

Discussion

Our results demonstrate the ability of SPIO nanoparticles and an MF to support normal SGN survival and growth, to promote neurite extension, to enhance neurite alignment, and to regulate cell migration in vitro. However, the biosafety of SPIO nanoparticles should be carefully evaluated

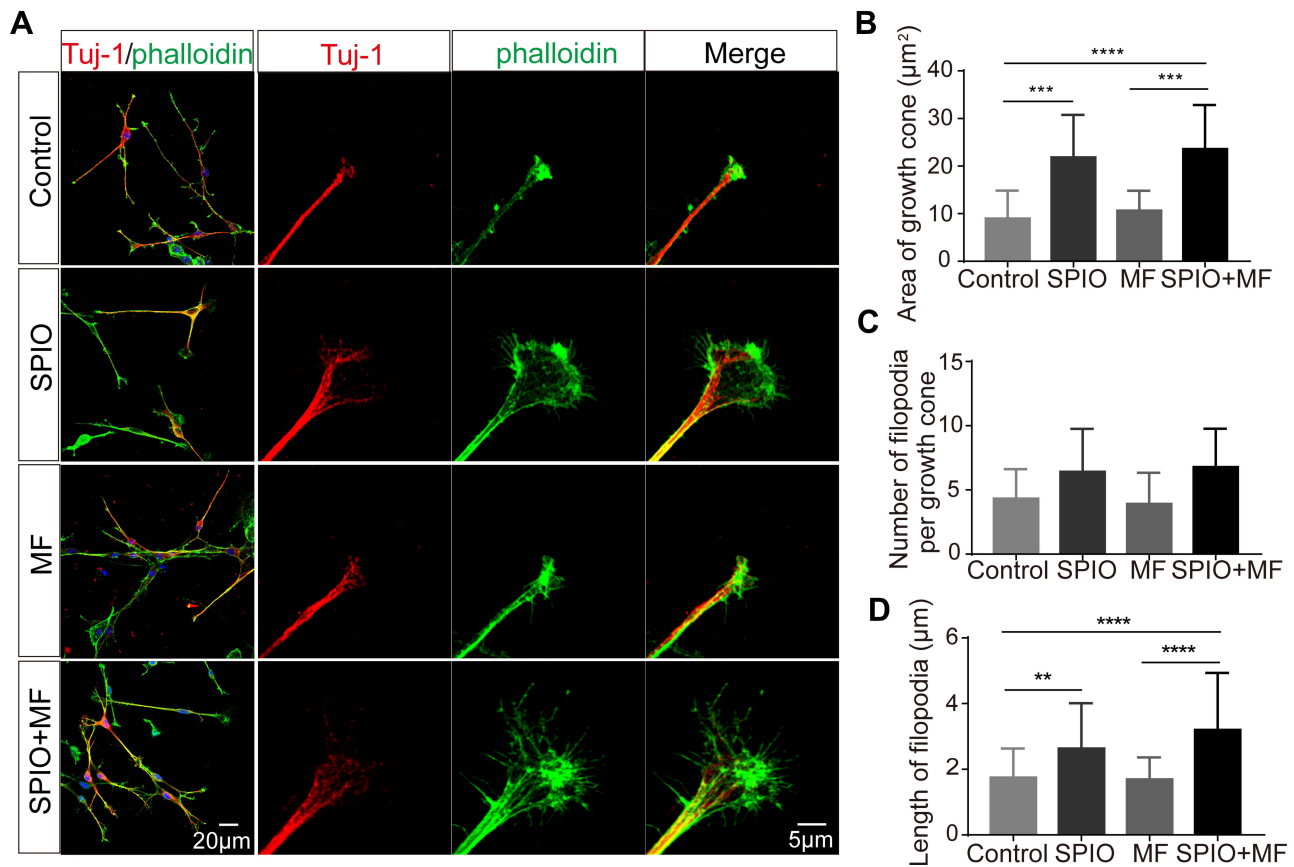


Figure 5 SPIO nanoparticles (100 µg/mL) and MF (80–90 mT) accelerated the development of SGN growth cones and filopodia. **(A)** Low-resolution and high-resolution confocal images of growth cones immunostained for βIII-tubulin (red) and phalloidin (green) to mark the F-actin structures. **(B)** Average growth cone area. ***p < 0.001, ****p < 0.0001 by one-way ANOVA. **(C)** Average number of filopodia emerging from the growth cones. No significant difference by one-way ANOVA. **(D)** Average length from the tips of each filopodium to the edge of the growth cone. **p < 0.01, ****p < 0.0001 by one-way ANOVA.

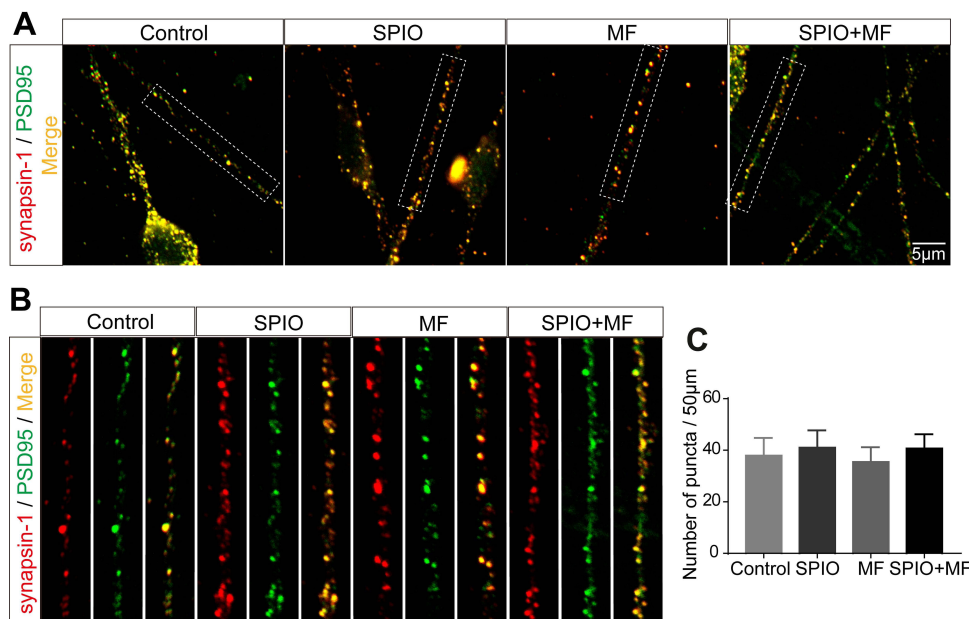


Figure 6 SPIO nanoparticles (100 µg/mL) and MF (80–90 mT) had no influence on the synapse density of SGNs. Low-resolution **(A)** and high-resolution **(B)** representative confocal images of synapses immunostained for synapsin-I and PSD95. **(C)** Average synapse density of SGNs. No significant differences by one-way ANOVA.

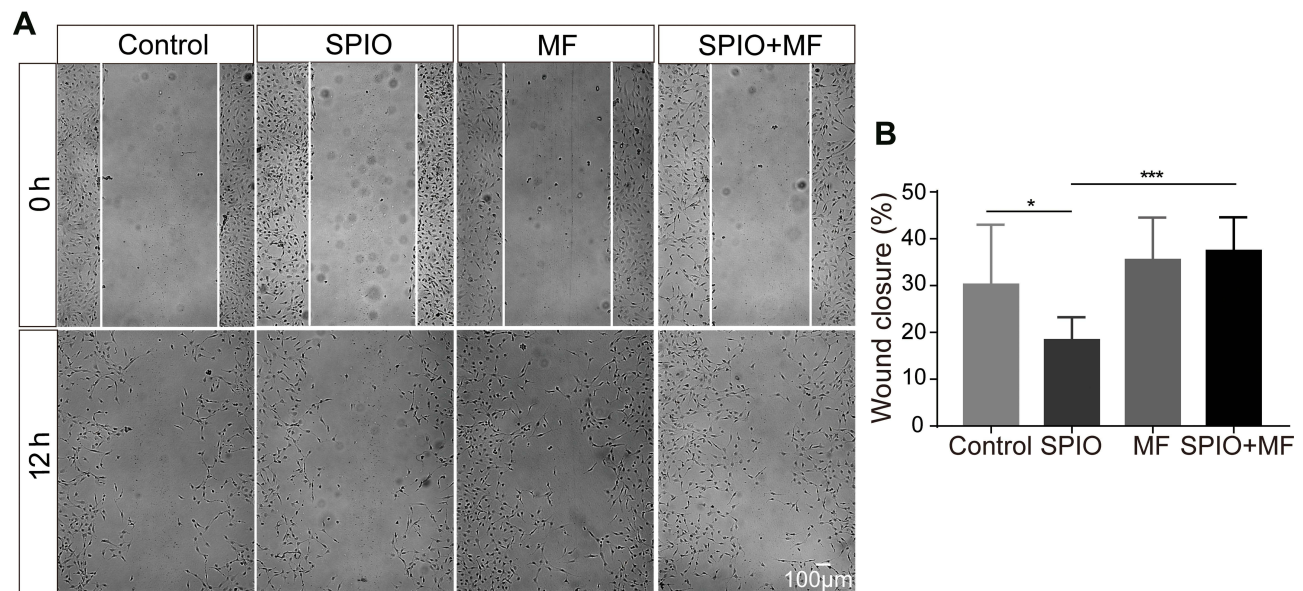


Figure 7 SPIO nanoparticles (100 $\mu\text{g}/\text{mL}$) and MF (80–90 mT) regulated the migration behavior of SGNs. **(A)** The wound healing assay showed the effects of SPIO nanoparticles and MF on SGN migration. **(B)** Histograms of the wound closure percentage in different groups. * $p < 0.05$, *** $p < 0.001$ by one-way ANOVA.

before further clinical application, and it is worth mentioning that we completely followed the technology used to produce Ferumoxytol – which is the only inorganic nano-drug approved by the FDA for clinical application – when preparing and synthesizing the SPIO nanoparticles. More importantly, the SPIO nanoparticles we synthesized have also been approved by the CFDA as an MRI agent and for iron supplementation, indicating the very high biosafety of the SPIO nanoparticles we used in our study. In this study, we demonstrated the good biocompatibility of SPIO nanoparticles with SGNs. In SGNs cultured with SPIO nanoparticles, the nanoparticles were localized in the cell body and neurites and showed no cytotoxicity at low concentrations. Similar results have been reported in studies evaluating the potential cytotoxicity of SPIO nanoparticles in different types of cells.^{31,35,36} Work by Liu et al suggested that there was no significant cytotoxicity of SPIO nanoparticles in dendritic cells when the cells were treated with 50 $\mu\text{g}/\text{mL}$ SPIO nanoparticles,³⁵ while our results showed that the SPIO nanoparticles had no cytotoxicity on SGNs at concentrations of 300 $\mu\text{g}/\text{mL}$, which showed better biocompatibility. In fact, the cytotoxicity of SPIO nanoparticles varies with particle size and cell type and is related to the type and stability of the nanoparticle coatings.³⁷ The SPIO nanoparticles we used in this work were coated with poly-L-lysine before incubating with SGNs, which should improve the biocompatibility of nanoparticles.

Our results show that SPIO nanoparticles and an MF promoted neurite growth and alignment. SPIO nanoparticles has the ability to promote the extension of SGN neurites, while the external MF is not a necessary condition for this. Although the underlying mechanisms responsible for the promotion of neurite growth by SPIO nanoparticles in nerve cells are still unclear, it has been presumed that Fe ions could be released from iron oxide nanoparticles inside the cells, which had the ability to enhance neurite outgrowth.³⁸ What's more, SPIO nanoparticles combined with an external MF was capable of guiding neurites to preferentially grow parallel to the direction of the MF. Similar results have been obtained in previous reports. Yuan et al found that SPIO-Au core-shell nanoparticles functionalized with nerve growth factor can accelerate the axonal growth of PC-12 cells and align the neurites with the direction of the applied magnetic force.³⁹ The alignment of the neurites can be attributed to the magnetic field acting on SPIO inside the neurite, and this makes it possible to manipulate and orient the neurites to achieve the desired orientation. In fact, more and more evidence shows that cellular tension is a critical factor in neuronal growth and development.⁴⁰ Mechanical interactions between physical cues and cells seem not only to be responsible for neurite growth, but also for the orientation of neurites, and our results also confirm that MFs promote neurite growth and orient the neurite growth of SGNs cultured with SPIOs. However, the MF intensity used in

this study was not high enough due to the limitations of the experimental setup. In the future, MFs with higher intensity should be used to investigate whether they have better orientation effects on cells. It would also be useful to determine the minimum MF intensity that can produce the results observed in this study. We believe that directing SGN neurite growth towards CI electrodes using MFs will be useful for promoting direct contacts between the cells and the electrodes of the implant. Such improved connections will increase the effectiveness of CIs as a treatment for sensorineural hearing loss.

The ability to control neuron migration has important potential in neural regeneration studies and therapies. Therefore, we performed a wound healing assay to assess whether the SPIO nanoparticles and an MF affect the migration of SGNs. We found that the SPIO nanoparticles significantly inhibited the migration of SGNs compared with untreated cells. However, compared with the SPIO group, SGNs that had internalized SPIO nanoparticles exhibited enhanced migration when an external MF was applied, which was comparable to the control group. Therefore, the reduced migration capacity caused by SPIO nanoparticles can be reversed by applying an external MF. Indeed, the influence of SPIO nanoparticles on the migration of different types of cells is still a matter of debate. Neural stem cells labeled with SPIO nanoparticles have been shown to reduce the migration capacity of cells,⁴¹ which is similar to what was observed in the present study. According to the results of Soenen et al, when SPIO nanoparticles were internalized, cellular actin cytoskeleton and microtubule networks will be destroyed, leading to loss of focal adhesion and decreased migration ability.⁴² In contrast, another study showed that the internalization of SPIO had no significant effect on the migration of Schwann cells compared to controls, although the application of an MF significantly enhanced the migration of Schwann cells toward the magnetic source.⁴³

The SPIO nanoparticles used in this study was synthesized using classical chemical co-precipitation methods, and these nanoparticles have been approved by the CFDA as an MRI agent and for iron supplementation, thus indicating their high level of safety. The viability assays performed in the present study confirm the excellent biocompatibility of SPIO nanoparticles. We furthermore demonstrated that the mechanical tension created by SPIO nanoparticles within an MF can promote neuron growth and guide the orientation of SGN neurites. We believe that future in vivo studies will reveal how neural

cells respond to complex mechanical environments. Together with previously published results, we think the results of the present study will be of great significance for nerve regeneration and recovery, and thus will lead to new strategies for the treatment of injured neurons and degenerative diseases, especially the treatment of sensorineural hearing loss caused by the degeneration of SGNs.

Data Sharing Statement

The data could be obtained upon reasonable request to the corresponding author (Dr. Mingliang Tang).

Funding

This work was supported by grants from the Major State Basic Research Development Program of China (973 Program) (2017YFA0104303), the National Natural Science Foundation of China (No. 81970883).

Disclosure

The authors report no conflicts of interest in this work.

References

- Coate TM, Kelley MW. Making connections in the inner ear: recent insights into the development of spiral ganglion neurons and their connectivity with sensory hair cells. *Semin Cell Dev Biol.* 2013;24:460–469. doi:10.1016/j.semcdb.2013.04.003
- Diaz RC. Inner ear protection and regeneration: a ‘historical’ perspective. *Curr Opin Otolaryngol Head Neck Surg.* 2009;17:363.
- Kujawa SG, Liberman MC. Adding insult to injury: cochlear nerve degeneration after “temporary” noise-induced hearing loss. *J Neurosci.* 2009;29:14077–14085. doi:10.1523/JNEUROSCI.2845-09.2009
- Poirrier AL, Van den Ackerveken P, Kim TS, et al. Ototoxic drugs: difference in sensitivity between mice and guinea pigs. *Toxicol Lett.* 2010;193:41–49. doi:10.1016/j.toxlet.2009.12.003
- Ding D, Allman BL, Salvi R. Review: ototoxic characteristics of platinum antitumor drugs. *Anat Rec (Hoboken).* 2012;295:1851–1867. doi:10.1002/ar.22577
- Kusunoki T, Cureoglu S, Schachern PA, et al. Age-related histopathologic changes in the human cochlea: a temporal bone study. *Otolaryngol Head Neck Surg.* 2004;131:897–903. doi:10.1016/j.otohns.2004.05.022
- Schuknecht HF, Gacek MR. Cochlear Pathology in Presbycusis. *Ann Otol Rhinol Laryngol.* 102:1–16. doi:10.1177/00034894931020S101
- Dabdoub A, Fritzsche B, Popper AN, et al. The primary auditory neurons of the mammalian cochlea. ed. 2016.
- Shepherd RK, Hardie NA. Deafness-induced changes in the auditory pathway: implications for cochlear implants. *Audiol Neurootol.* 2001;6:305–318. doi:10.1159/000046843
- Zeng FG, Rebscher S, Harrison W, et al. Cochlear implants: system design, integration, and evaluation. *IEEE Rev Biomed Eng.* 2008;1:115–142. doi:10.1109/RBME.2008.2008250
- Tong M, Brugeaud A, Edge AS. Regenerated synapses between postnatal hair cells and auditory neurons. *J Assoc Res Otolaryngol.* 2013;14:321–329. doi:10.1007/s10162-013-0374-3

12. Hahnwald S, Tschertner A, Marconi E, et al. Response profiles of murine spiral ganglion neurons on multi-electrode arrays. *J Neural Eng.* 2016;13:016011. doi:10.1088/1741-2560/13/1/016011
13. Cheng EL, Leigh B, Guymon CA, et al. Quantifying spiral ganglion neurite and schwann behavior on micropatterned polymer substrates. *Methods Mol Biol.* 2016;1427:305–318.
14. Van Essen DC. A tension-based theory of morphogenesis and compact wiring in the central nervous system. *Nature.* 1997;385:313–318. doi:10.1038/385313a0
15. Heidemann SR, Buxbaum RE. Mechanical tension as a regulator of axonal development. *Neurotoxicology.* 1994;15:95–107.
16. Flanagan LA, Ju YE, Marg B, et al. Neurite branching on deformable substrates. *Neuroreport.* 2002;13:2411–2415. doi:10.1097/00001756-200212200-00007
17. Xue J, Georges PC, Li B, et al. Cell growth in response to mechanical stiffness is affected by neuron- astroglia interactions. *Open Neurosci J.* 2007;107:7–14.
18. Lalande C, Miraux S, Derkaoui SM, et al. Magnetic resonance imaging tracking of human adipose derived stromal cells within three-dimensional scaffolds for bone tissue engineering. *Eur Cell Mater.* 2011;21:341–354. doi:10.22203/eCM.v021a25
19. Yoffe S, Leshuk T, Everett P, et al. Superparamagnetic iron oxide nanoparticles (SPIONs): synthesis and surface modification techniques for use with MRI and other biomedical applications. *Curr Pharm Des.* 2013;19:493–509. doi:10.2174/138161213804143707
20. Nam SY, Ricles LM, Suggs LJ, et al. Imaging strategies for tissue engineering applications. *Tissue Eng Part B Rev.* 2015;21:88–102. doi:10.1089/ten.teb.2014.0180
21. Ramaswamy S, Greco JB, Uluer MC, et al. Magnetic resonance imaging of chondrocytes labeled with superparamagnetic iron oxide nanoparticles in tissue-engineered cartilage. *Tissue Eng Part A.* 2009;15:3899–3910. doi:10.1089/ten.tea.2008.0677
22. Saldanha KJ, Doan RP, Ainslie KM, et al. Micrometer-sized iron oxide particle labeling of mesenchymal stem cells for magnetic resonance imaging-based monitoring of cartilage tissue engineering. *Magn Reson Imaging.* 2011;29:40–49. doi:10.1016/j.mri.2010.07.015
23. Singh N, Jenkins GJ, Asadi R, et al. Potential toxicity of superparamagnetic iron oxide nanoparticles (SPION). *Nano Rev.* 2010;1.
24. Andreu I, Natividad E, Solozabal L, et al. Nano-objects for addressing the control of nanoparticle arrangement and performance in magnetic hyperthermia. *ACS Nano.* 2015;9:1408–1419. doi:10.1021/nn505781f
25. Vu-Quang H, Yoo MK, Jeong HJ, et al. Targeted delivery of mannan-coated superparamagnetic iron oxide nanoparticles to antigen-presenting cells for magnetic resonance-based diagnosis of metastatic lymph nodes in vivo. *Acta Biomater.* 2011;7:3935–3945. doi:10.1016/j.actbio.2011.06.044
26. Mashhadi Malekzadeh A, Ramazani A, Tabatabaei Rezaei SJ, et al. Design and construction of multifunctional hyperbranched polymers coated magnetite nanoparticles for both targeting magnetic resonance imaging and cancer therapy. *J Colloid Interface Sci.* 2017;490:64–73. doi:10.1016/j.jcis.2016.11.014
27. Alimohammadi S, Salehi R, Amini N, et al. Synthesis and physico-chemical characterization of biodegradable plga-based magnetic nanoparticles containing amoxicillin. *Bulletin- Korean Chem Soc.* 2012;33:3225–3232. doi:10.5012/bkcs.2012.33.10.3225
28. Nguyen D, Pham BTT, Huynh V, et al. Monodispersed polymer encapsulated superparamagnetic iron oxide nanoparticles for cell labeling. *Polymer.*
29. Marcus M, Karni M, Baranes K, et al. Iron oxide nanoparticles for neuronal cell applications: uptake study and magnetic manipulations. *J Nanobiotechnol.* 2016;14:37. doi:10.1186/s12951-016-0190-0
30. Riggio C, Calatayud MP, Giannaccini M, et al. The orientation of the neuronal growth process can be directed via magnetic nanoparticles under an applied magnetic field. *Nanomedicine.* 2014;10:1549–1558. doi:10.1016/j.nano.2013.12.008
31. Wang P, Ma S, Ning G, et al. Entry-Prohibited Effect of kHz pulsed magnetic field upon interaction between spio nanoparticles and mesenchymal stem cells. *IEEE Trans Biomed Eng.* 2020;67:1152–1158. doi:10.1109/TBME.2019.2931774
32. Liu T, Jin L, Lu W, et al. Sequence-dependent synergistic cytotoxicity of icotinib and pemetrexed in human lung cancer cell lines in vitro and in vivo. *J Exp Clin Cancer Res.* 2019;38:148. doi:10.1186/s13046-019-1133-z
33. Chen B, Guo Z, Guo C, et al. Moderate cooling coprecipitation for extremely small iron oxide as a pH dependent T1-MRI contrast agent. *Nanoscale.* 2020;12:5521–5532. doi:10.1039/C9NR10397J
34. Meyer D, Bonhoeffer T, Scheuss V. Balance and stability of synaptic structures during synaptic plasticity. *Neuron.* 2014;82:430–443. doi:10.1016/j.neuron.2014.02.031
35. Liu H, Dong H, Zhou N, et al. SPIO Enhance the Cross-Presentation and Migration of DCs and Anionic SPIO Influence the Nanoadjuvant Effects Related to Interleukin-1beta. *Nanoscale Res Lett.* 2018;13:409. doi:10.1186/s11671-018-2802-0
36. Egawa EY, Kitamura N, Nakai R, et al. A DNA hybridization system for labeling of neural stem cells with SPIO nanoparticles for MRI monitoring post-transplantation. *Biomaterials.* 2015;54:158–167. doi:10.1016/j.biomaterials.2015.03.017
37. Gupta AK, Gupta M. Cytotoxicity suppression and cellular uptake enhancement of surface modified magnetic nanoparticles. *Biomaterials.* 2005;26(13):1565–1573. doi:10.1016/j.biomaterials.2004.05.022
38. Kim JA, Lee N, Kim BH, et al. Enhancement of neurite outgrowth in PC12 cells by iron oxide nanoparticles. *Biomaterials.* 2011;32:2871–2877. doi:10.1016/j.biomaterials.2011.01.019
39. Yuan M, Wang Y, Qin YX. Promoting neuroregeneration by applying dynamic magnetic fields to a novel nanomedicine: superparamagnetic iron oxide (SPIO)-gold nanoparticles bounded with nerve growth factor (NGF). *Nanomedicine.* 2018;14:1337–1347. doi:10.1016/j.nano.2018.03.004
40. Franze K, Guck J. The biophysics of neuronal growth. *Rep Prog Phys.* 2010;73(9):94600–94601. doi:10.1088/0034-4885/73/9/094601
41. Cromer Berman SM, Kshitiz WCJ. Cell motility of neural stem cells is reduced after SPIO-labeling, which is mitigated after exocytosis. *Magn Reson Med.* 2013;69:255–262. doi:10.1002/mrm.24216
42. Soenen SJ, Himmelreich U, Nuytten N, et al. Cytotoxic effects of iron oxide nanoparticles and implications for safety in cell labelling. *Biomaterials.* 2011;32:195–205. doi:10.1016/j.biomaterials.2010.08.075
43. Huang L, Xia B, Liu Z, et al. Superparamagnetic iron oxide nanoparticle-mediated forces enhance the migration of schwann cells across the astrocyte-schwann cell boundary in vitro. *Front Cell Neurosci.* 2017;11:83. doi:10.3389/fncel.2017.00083

International Journal of Nanomedicine

Dovepress

Publish your work in this journal

The International Journal of Nanomedicine is an international, peer-reviewed journal focusing on the application of nanotechnology in diagnostics, therapeutics, and drug delivery systems throughout the biomedical field. This journal is indexed on PubMed Central, MedLine, CAS, SciSearch[®], Current Contents[®]/Clinical Medicine,

Journal Citation Reports/Science Edition, EMBase, Scopus and the Elsevier Bibliographic databases. The manuscript management system is completely online and includes a very quick and fair peer-review system, which is all easy to use. Visit <http://www.dovepress.com/testimonials.php> to read real quotes from published authors.

Submit your manuscript here: <https://www.dovepress.com/international-journal-of-nanomedicine-journal>